

Solar Oscillations

A. G. Kosovichev

HEPL, Stanford University, Stanford, CA 94305

Abstract. In recent years solar oscillations have been studied in great detail, both observationally and theoretically; so, perhaps, the Sun currently is the best understood pulsating star. The observational studies include long, almost uninterrupted series of oscillation data from the SOHO spacecraft and ground-based networks, GONG and BiSON, and more recently, extremely high-resolution observations from the Hinode mission. These observational data cover the whole oscillation spectrum, and have been extensively used for helioseismology studies, providing frequencies and travel times for diagnostics of the internal stratification, differential rotation, zonal and meridional flows, subsurface convection and sunspots. Together with realistic numerical simulations they lead to better understanding of the excitation mechanism and interactions of the oscillations with turbulence and magnetic fields. However, many problems remain unsolved. In particular, the precision of the helioseismology measurements is still insufficient for detecting the dynamo zone and deep routes of sunspots. Our knowledge of the oscillation physics in strong magnetic field regions is inadequate for interpretation of MHD waves in sunspots and for sunspot seismology. A new significant progress in studying the solar oscillations is expected from the Solar Dynamics Observatory scheduled for launch in 2010.

Keywords: solar oscillations, helioseismology, solar interior

PACS: <Replace this text with PACS numbers; choose from this list: <http://www.aip.org/pacs/index.html>>

INTRODUCTION

Solar oscillations have been studied extensively since their discovery by Leighton et al. [1]. Currently, it is well-understood that the 5-min oscillations that dominate the dynamics of the solar atmosphere represent radial and non-radial acoustic and surface gravity modes stochastically excited by turbulent convection and trapped below the surface. In addition, impulsive localized excitation by solar flares has been observed in several cases. The solar oscillation modes are observed in a wide range of angular degree, from 0 to 3000, and used to infer the internal structure and dynamics of the Sun by methods of helioseismology. These methods are generally divided into two classes: global and local helioseismology.

Global helioseismology uses measurements of normal mode frequencies and is based on the classical theory of stellar oscillations [3]. This theory provides relationships between normal modes frequencies and interior properties such as the radial and latitudinal distributions of the sound speed, density and angular velocity. Local helioseismology measures local 3D perturbations of the sound speed and flow fields associated with large-scale solar convection and magnetic structures. These methods are based on measurements of wave dispersion properties (e.g. frequency shifts in local areas) and wave travel times. Theoretical description of these techniques is more complicated than for the global methods, and is still being developed. The main complexity comes from the need to take into account coupling among the normal modes caused by 3D perturbation. Global helioseismol-

ogy analyses generally ignore this coupling and consider only frequency shifts and splitting caused by spherical and axisymmetrical (and also North-south symmetrical) perturbations. While the axisymmetrical approximation only crudely describes the structure and dynamics of the Sun the global helioseismology methods are currently the main tool for probing the deep interior and variations in the convection zone associated with the solar activity cycle. Three-dimensional local helioseismology methods are still limited to diagnostics of relatively shallow subsurface layers. However, some initial attempts have been made to probe the structure of the tachocline (a transition layer between the radiative core and the convective envelope) by a time-distance helioseismology method [4].

While the physics of solar oscillations and their mechanism are generally understood many interesting and important details are still unknown. Among these are the precise nature of turbulent perturbations that drive solar oscillations, mechanisms of asymmetry of the oscillation line profiles in the observed power spectrum, phase and amplitude relations between velocity and intensity oscillations, the role of magnetic fields in the mode excitation and properties, as well as non-adiabatic effects caused by interaction of waves with turbulence and radiation. Also, the mechanism of flare-excited oscillation ("sunquakes") is not well-understood.

Knowing the physics of solar oscillations is very important for improving the accuracy of helioseismic measurements. For instance, initially, frequencies of normal modes were measured by fitting a symmetrical Lorentzian profile to the peaks in the oscillation power

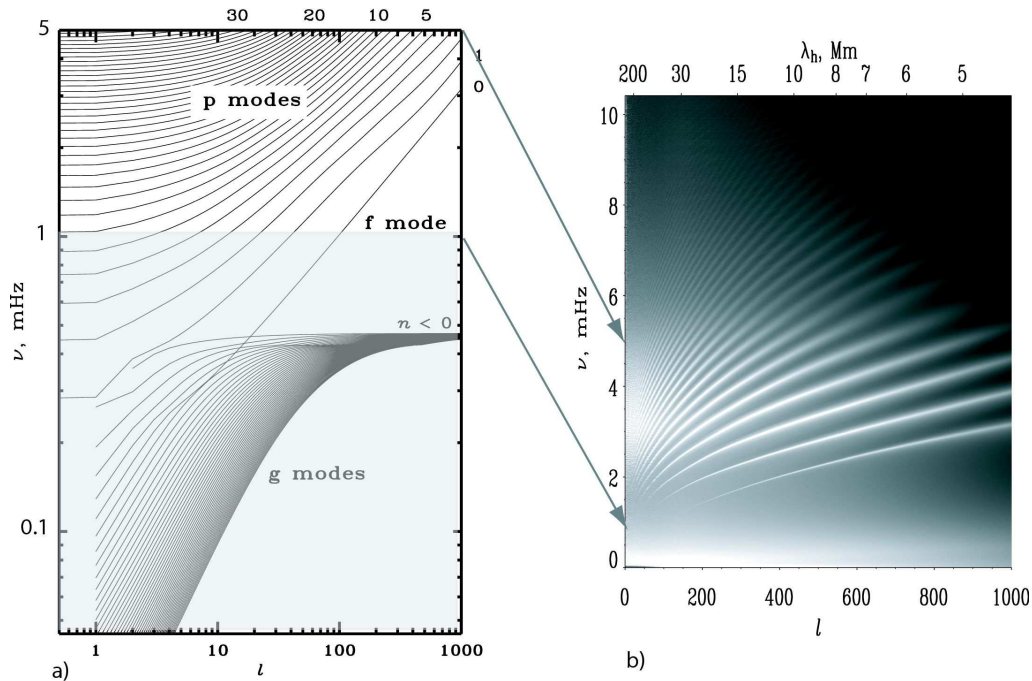


FIGURE 1. a) Theoretical spectrum of solar oscillations [2]. b) The power spectrum of solar oscillations observed from SOHO/MDI.

spectra. This profile comes from a simplified model that treats the oscillation modes as a damping harmonic oscillator (e.g. [5]). However, this results in systematic frequency shifts because the lines are asymmetrical. Thus, more recent measurements are carried out using asymmetrical profiles [6]. Also, accurate models of the excitation source are required for calculating sensitivity functions for acoustic travel times using a Born approximation in time-distance helioseismology [7, 8]. For this type of measurements it is particularly important to take into account variations of the strength and spectral distribution in magnetic regions. In an extreme case of sunspot umbra the excitation of acoustic waves is suppressed because the strong magnetic field inhibits convection. The spatial and spectral variations of the oscillation power may cause systematic shifts in travel-time measurements when a phase-speed filtering procedure to improve the signal-to-noise ratio is applied [9, 10]. Thus, the current research in the field of solar oscillations is focused on improving the understanding of the excitation mechanism, effects of magnetic fields on wave excitation, propagation and damping, and also on developing more accurate methods of helioseismology, particularly, the local techniques. This article presents a brief overview of some aspects of the solar oscillation physics and helioseismology methods, but no means this is a comprehensive literature review.

PHYSICS OF SOLAR OSCILLATIONS

Oscillation Power Spectrum

The theoretical spectrum of solar oscillation modes shown in Fig. 1a covers a wide range of frequencies and angular degrees. It includes oscillations of three types: acoustic (p) modes, surface gravity (f) modes and internal gravity (g) modes. In this spectrum each curve corresponds to a specific overtone of non-radial modes, which can be described by the number of nodes along the radius (or by the radial order, n). The angular degree, l , of corresponding spherical harmonics describes the horizontal wave number (or inverse horizontal wavelength). The p-modes cover the frequency range from 0.3 to 5 mHz (or from 3 to 55 min in oscillation periods). The low frequency limit corresponds to the first radial harmonic, and the upper limit is set by the acoustic cut-off frequency of the solar atmosphere. The g-modes have an upper limit corresponding to the maximum Brünt-Väisälä frequency (~ 0.45 mHz) in the radiative zone and occupy the low-frequency part of the spectrum. The intermediate frequency range of 0.3-0.4 mHz at low angular degrees is a region of mixed modes. These modes behave like g-mode in the deep interior and like p-modes in the outer region. The apparent crossings in this diagram are not the actual crossings: the mode branches become close in frequencies but do not cross. A similar phenomenon is

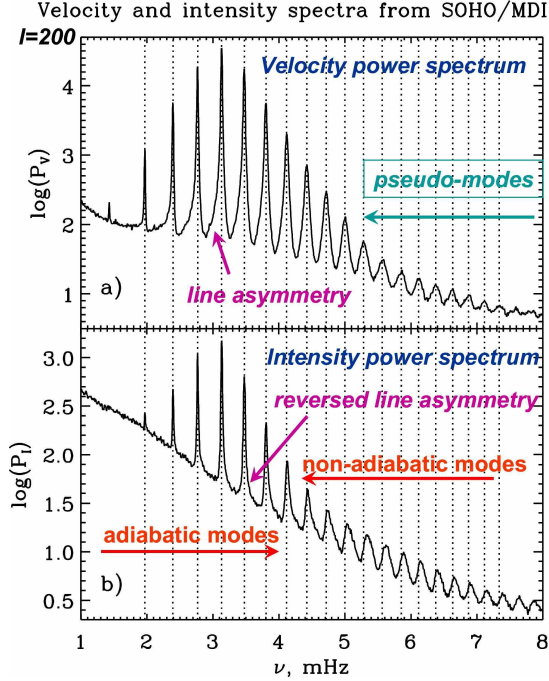


FIGURE 2. Power spectra of $l = 200$ mode obtained from SOHO/MDI observations of a) Doppler velocity, b) continuum intensity. [19]

known in quantum mechanics as avoided crossing.

So far, only the upper part of the solar oscillation spectrum is observed. The lowest frequencies of detected p- and f-modes are of about 1 mHz. Below this frequency the mode amplitudes decrease below the noise level, and become unobservable. There have been several attempts to identify low-frequency p-modes or even g-modes in the noisy spectrum, but so far these results are not convincing.

The observed power spectrum is shown in Fig. 1b. The lowest ridge is the f-mode, and the other ridges are p-modes of the radial order, n , starting from $n = 1$. The ridges of the oscillation modes disappear in the convective noise at frequencies below 1 mHz. At low angular degrees only high- n modes are observed. However, the n -values of these modes can be easily determined by tracing the high- n ridges of the high-degree modes into the low-degree region. This provides unambiguous identification of the low-degree solar modes. Obviously, the mode identification is much more difficult for spatially unresolved oscillations of other stars.

Excitation Mechanism

Solar oscillations are driven by turbulent convection in a shallow subsurface superadiabatic layer where con-

vective velocities are the highest. However, details of the stochastic excitation mechanism are not fully established. Solar convection in the superadiabatic layer forms small-scale granulation cells. Analysis of observations and numerical simulations has shown that sources of solar oscillations are associated with strong downdrafts in dark intergranular lanes [13]. These downdrafts are driven by radiative cooling and may reach near-sonic velocity of several km/s. This process has features of convective collapse [14].

Calculations of the work integral for acoustic modes using the realistic numerical simulations of Stein and Nordlund [15] have shown that the principal contribution to the mode excitation is provided by turbulent Reynolds stresses and that a smaller contribution comes from non-adiabatic pressure fluctuations.

As we have pointed out observations show that the modal lines in the oscillation power spectrum are not Lorentzian but display a strong asymmetry [16, 17]. Curiously, the asymmetry has the opposite sense in the power spectra calculated from Doppler velocity and intensity oscillations. The asymmetry itself can be easily explained by interference of waves emanated by a localized source [18], but the asymmetry reversal is surprising and indicates on complicated radiative dynamics of the excitation process, and is still not fully understood. However, it is clear that the line shape of the oscillation modes and the phase-amplitude relations of the velocity and intensity oscillations carry substantial information about the excitation mechanism and, thus, require careful data analysis and modeling.

Line Asymmetry and Pseudo-modes

Figure 2 shows the oscillation power spectrum of $l = 200$ mode, obtained from the SOHO/MDI Doppler velocity and intensity data. The line asymmetry is apparent, particularly, at low frequencies. In the velocity spectrum, there is more power in the low-frequency wings than in the high-frequency wings of the spectral lines. In the intensity spectrum the distribution of power is reversed. The data also show that the asymmetry varies with frequency. It is the strongest for the f-mode and low-frequency p-mode peaks. At higher frequencies the peaks become more symmetrical, and extend well above the acoustic cut-off frequency, which is about 5 mHz.

Acoustic waves with frequencies below the cut-off frequency are completely reflected by the surface layers because of the steep density gradient. These waves are trapped in the interior, and their frequencies are determined by the resonant conditions, which depend on the solar structure. But the waves with frequencies above the cut-off frequency escape into the solar atmosphere.

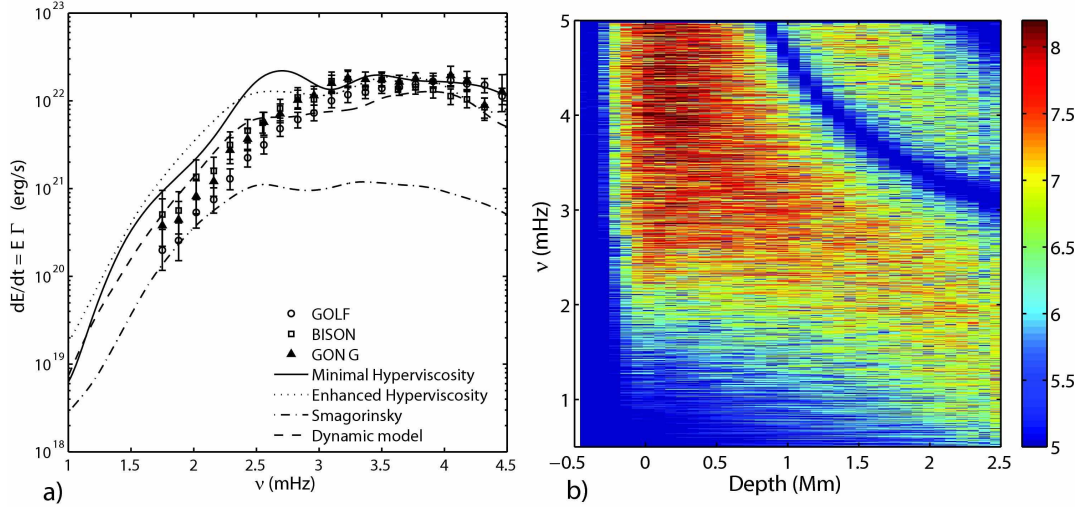


FIGURE 3. a) Comparison of observed and calculated rate of stochastic energy input to modes for the entire solar surface (erg.s^{-1}). Observed distributions: *circles* SoHo-GOLF, *squares* BISON, and *triangles* GONG for $l = 1$ [11]. b) Logarithm of the work integrand in units of $\text{erg.cm}^{-2}.\text{s}^{-1}$, as a function of depth and frequency for numerical simulations with the dynamic turbulence model. [12]

Above this frequency the power spectrum peaks correspond to so-called "pseudo-modes". These are caused by constructive interference of acoustic waves excited by the sources located in the granulation layer traveling upward and the waves traveling downward, reflected in the deep interior and arriving back to the surface. Frequencies of these modes are no longer determined by the resonant conditions of the solar structure. They depend on the location and properties of the excitation source ("source resonance"). The pseudo-mode peaks in the velocity and intensity power spectra are shifted relative to each other by almost a half-width. They are also slightly shifted relative to the normal mode peaks despite they look like a continuation of the normal-mode ridges in Figs 1b and 4a. This happens because the excitation sources are located in a shallow subsurface layer, which is very close to the reflection layers of the normal modes. Changes in the frequency distributions below and above the acoustic cut-off frequency can be easily noticed by plotting the frequency differences along the modal ridges.

The asymmetrical profiles of normal-mode peaks are also caused by the localized excitation sources. The interference signal between acoustic waves traveling from the source upwards and the waves traveling from the source downward and coming back to the surface after the internal reflection depends on the wave frequency. Depending on the source (multipole) type the interference signal can be stronger at frequencies lower or higher the resonant normal frequencies, thus resulting in asymmetry in the power distribution around the resonant peak. Calculations of Nigam et al [19] showed that the asymmetry observed in the velocity spectra and the distribution of

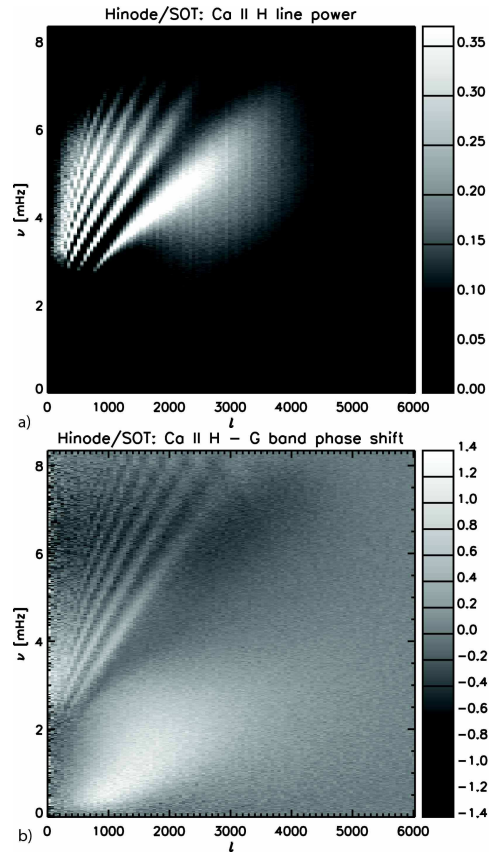


FIGURE 4. a) The oscillation power spectrum from Hinode CaII H line observations. b) The phase shift between CaII H and G-band (units are in radians). [20]

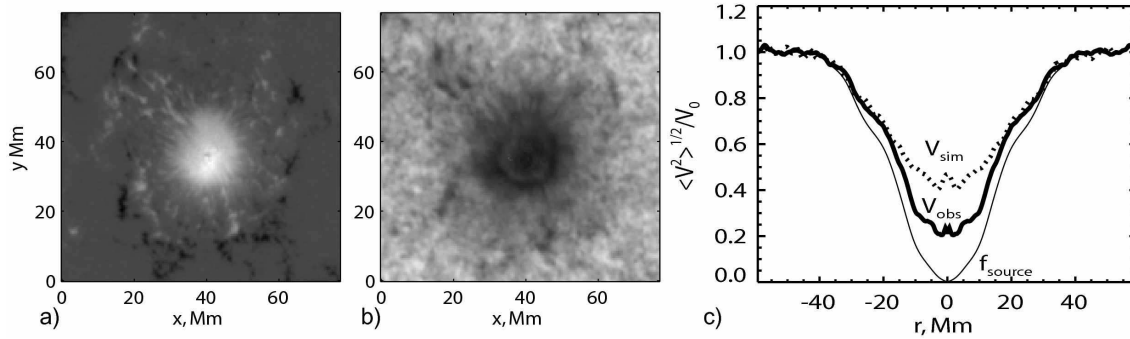


FIGURE 5. a) Line-of-sight magnetic field map of a sunspot (AR8243); b) oscillation amplitude map; c) profiles of rms oscillation velocities at frequency 3.65 mHz for observations (thick solid curves) and simulations (dashed curves); the thin solid curve shows the distribution of the simulated source strength.[21]

the pseudo-mode peaks can be explained by a composite source consisting of a monopole term (mass term) and a dipole term (force due to Reynolds stress) located in the zone of superadiabatic convection at a depth of 75 ± 50 km below the photosphere. In this model the reversed asymmetry in the intensity power spectra is explained by effects of a correlated noise added to the oscillation signal through fluctuations of solar radiation during the excitation process. Indeed, if the excitation mechanism is associated with the high-speed turbulent downdrafts in dark lanes of granulation the local darkenings contribute to the intensity fluctuations caused by excited waves. The model also explains the shifts of pseudo-mode frequency peaks and their higher amplitude in the intensity spectra.

While this scenario looks plausible and qualitatively explains the main properties of the power spectra details of the physical processes are still uncertain. In particular, it is unclear whether the correlated noise affects only the intensity signal or both the intensity and velocity. It has been suggested that the velocity signal may have a correlated contribution due to convective overshoot [22]. Attempts to estimate the correlated noise components from the observed spectra have not provided conclusive results [23, 24]. Realistic numerical simulations [25] have reproduced the observed asymmetries and provided an indication that radiation transfer plays a critical role in the asymmetry reversal.

Recent high-resolution observations of solar oscillation simultaneously in two intensity filters, in molecular G-band and CaII H line, from the Hinode space mission [26, 27] revealed significant shifts in frequencies of pseudo-modes observed in the CaII H and G-band intensity oscillations [20]. The phase of the cross-spectrum of these oscillations shows peaks associated with the p-mode lines but no phase shift for the f-mode (Fig. 4b). The p-mode properties can be qualitatively reproduced in a simple model with a correlated background if the correlated noise level in the Ca II H data is higher than

in the G-band data [20]. Perhaps, the same effect can explain also the frequency shift of pseudo-modes. The CaII H line is formed in the lower chromosphere while the G-band signal comes from the photosphere. But how this may lead to different levels of the correlated noise is unclear.

The Hinode results suggest that multi-wavelength observations of solar oscillations, in combination with the traditional intensity-velocity observations, may help to determine the level of the correlated background noise and to determine the type of wave excitation sources on the Sun.

In addition, Hinode provided observations of non-radial acoustic and surface gravity modes of very high angular degree. These observations show that the oscillation ridges are extended up to $l \simeq 4000$ (Fig. 4a). In the high-degree range, $l \geq 2500$ frequencies of all oscillations exceed the acoustic cut-off frequency. The line width of these oscillations dramatically increases, probably, due to strong scattering on turbulence [29]. Nevertheless, the ridge structure extending up to 8 mHz (Nyquist frequency of these observations) is quite clear. Although the ridge slope clearly changes at the transition from the normal modes to the pseudo-modes.

Magnetic Effects

In general, the main factors causing variations in oscillation properties in magnetic regions, can be divided in two types: direct and indirect. The direct effects are due to additional magnetic restoring forces that can change the wave speed and may transform acoustic waves into different types of MHD waves. The indirect effects are caused by changes in convective and thermodynamic properties in magnetic regions. These include depth-dependent variations of temperature and density, large-scale flows, and changes in wave source distribution and

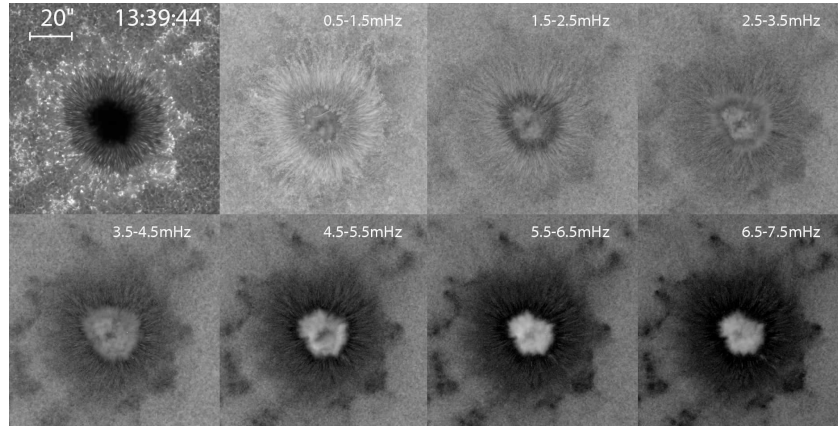


FIGURE 6. CaII H intensity image from Hinode observations (top-left) and the corresponding power maps from CaII H intensity data in five frequency intervals of active region NOAA 10935. The field of view is 100 arcsec square in all the panels. The power is displayed in logarithmic greyscaling. [28].

strength. Both direct and indirect effects may be present in observed properties such as oscillation frequencies and travel times, and often cannot be easily disentangled by data analyses causing confusions and misinterpretations. Also, one should keep in mind that simple models of MHD waves derived for various uniform magnetic configurations and without stratification may not provide correct explanations to solar phenomena. In this situation, numerical simulations play an important role in investigations of magnetic effects.

Observed changes of oscillation amplitude and frequencies in magnetic regions are commonly explained as a result of wave scattering and conversion into various MHD modes. However, recent numerical simulations helped to understand that magnetic fields not only affect the wave dispersion properties but also the excitation mechanism. In fact, changes in excitation properties of turbulent convection in magnetic regions may play a dominant role in observed phenomena.

Sunspot oscillations

For instance, it is well-known that the amplitude of 5-min oscillations is substantially reduced in sunspots. Observations show that more waves are coming into the sunspot than going out of the sunspot area (e.g. [30]). This is often attributed to absorption of acoustic waves in magnetic field due to conversion into slow MHD modes traveling along the field lines (e.g. [31]). However, since convective motions are inhibited by strong magnetic field of sunspots the excitation mechanism is also suppressed. Three-dimensional numerical simulations of this effect have shown that the reduction of acoustic emissivity can explain at least 50% of the observed power deficit in sunspots (Fig. 5) [10].

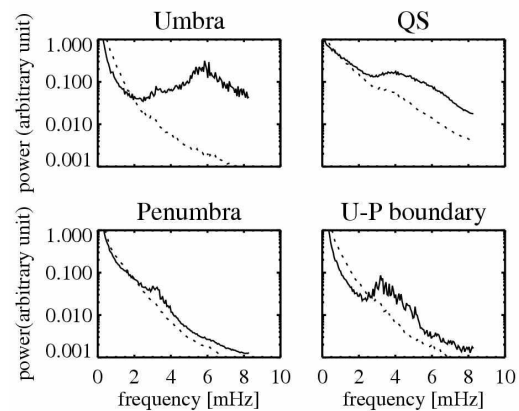


FIGURE 7. Power spectra averaged in the umbra (upper left), in the quiet region (upper right), in the penumbra (lower left), and around the boundary between the umbra and the penumbra (lower right). The CaII H (solid) and the G-band (dotted) intensity power spectra are shown. The ordinate is in an arbitrary unit in logarithmic scale.[28]

Another significant contribution comes from the amplitude changes caused by variations in the background conditions. Inhomogeneities in the sound speed may increase or decrease the amplitude of acoustic wave traveling through these inhomogeneities. Numerical simulations of MHD waves using magnetostatic sunspot models show that the amplitude of acoustic waves traveling through sunspot decreases when the wave is inside sunspot and then increases when the wave comes out of sunspot [32]. Simulations with multiple random sources show that these changes in the wave amplitude together with the suppression of acoustic sources can completely explain the observed deficit of the power of 5-min oscillations. Thus, the role of the MHD mode conversion

may be insignificant for explaining the power deficit of 5-min photospheric oscillations in sunspots. However, the mode conversion is expected to be significant higher in the solar atmosphere where magnetic forces become dominant.

We should note that while the 5-min oscillations in sunspots come mostly from outside sources there are also 3-min oscillations, which are probably intrinsic oscillations of sunspots. The origin of these oscillations is not yet understood. They are probably excited by a different mechanism operating in strong magnetic field.

Hinode observations added new puzzles to sunspot oscillations. Figure 6 shows a sample Ca II H intensity and the relative intensity power maps averaged over 1 mHz intervals in the range from 1 mHz to 7 mHz with logarithmic greyscaling [28]. In the Ca II H power maps, in all the frequency ranges, there is a small area (~ 6 arcsec in diameter) near the center of the umbra where the power was suppressed. This type of ‘node’ has not been reported before. Possibly, stable high-resolution observation made by Hinode/SOT was required to find such a tiny node, although analysis of other sunspots indicates that probably only a particular type of sunspots, e.g., round ones with axisymmetric geometry, exhibit such node-like structure. Above 4 mHz in the Ca II H power maps, power in the umbra is remarkably high. In the power maps averaged over narrower frequency range (0.05 mHz wide, not shown), the region with high power in the umbra seems to be more patchy. This may correspond to elements of umbral flashes, probably caused by overshooting convective elements [33]. The Ca II H power maps show a bright ring in the penumbra at lower frequencies. It probably corresponds to the running penumbral waves.

Figure 7 shows the power spectra of the G-band and the Ca II H intensity oscillations averaged in the quiet region, and sunspot penumbra, umbra and a transition area between the umbra and penumbra. In all these regions, the G-band intensity power decreases almost monotonically with the frequency, except the broad peak around 4 mHz in the quiet region. This peak corresponds to the global five-minute oscillation. The Ca II H intensity power in the quiet region shows the similar trend, while the power spectrum in the penumbra exhibits monotonic decrease, as is expected from the power maps (Fig. 6), except the narrow peak at 3 mHz. The Ca II H intensity power spectrum in the umbra has two peaks: one around 3 mHz and the other around 5.5 mHz. In the previous works (e.g. a review by [34], the dominant period of oscillation in the chromosphere was above 5.5 mHz, and, in contrast to our results, no significant power peaks were found in the 3 mHz range. The broad peak in the umbra-penumbra transition region, between 2 mHz and 5 mHz, is caused by running penumbral waves.

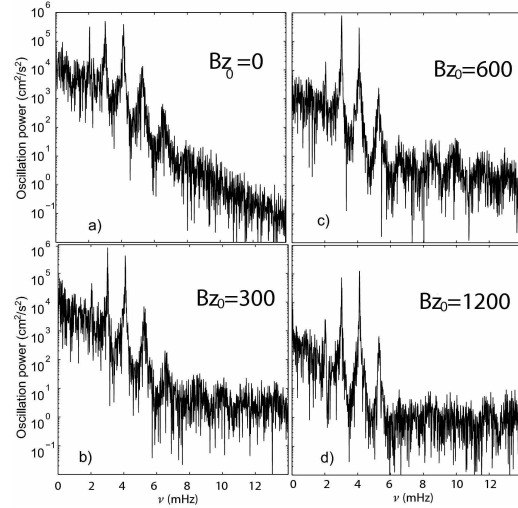


FIGURE 8. Power spectra of the horizontally averaged vertical velocity at the visible surface for different initial vertical magnetic fields. The peaks on the top of the smooth background spectrum of turbulent convection represent oscillation modes: the sharp asymmetric peaks below 6 mHz are resonant normal modes, while the broader peaks above 6 mHz, which become stronger in magnetic regions, correspond to pseudo-modes.[36]

Acoustic Halos

In moderate field regions, such as plages around sunspot regions observations reveal enhanced emission at high frequencies, 5-7 mHz, (with period ~ 3 min) [35]. Sometimes this emission is called "acoustic halo". Radiative MHD simulations of solar convection [36] in the presence of vertical magnetic field have shown that the magnetic field significantly changes the structure and dynamics of granulations, and thus the conditions of wave excitation. In magnetic field the granules become smaller, and the turbulence spectrum is shifted towards higher frequencies. This is illustrated in Figure 8, which shows the frequency spectrum of the horizontally averaged vertical velocity. Without magnetic field the turbulence spectrum declines sharply at the frequencies above 5 mHz, but in the presence of magnetic field it develops a plateau. In the plateau region characteristic peaks (corresponding to the "pseudo-modes") appear in the spectrum for moderate magnetic field strength of about 300-600 G. These peaks may explain the effect of "acoustic halo". Of course, more detailed theoretical and observational studies are required to confirm this mechanism. In particular, multi-wavelength observations of solar oscillations at several different heights would be important. Investigations of the excitation mechanism in magnetic regions is also important for interpretation of the variations of the frequency spectrum of low-degree modes on the Sun, and for asteroseismic diagnostics of stellar activity.

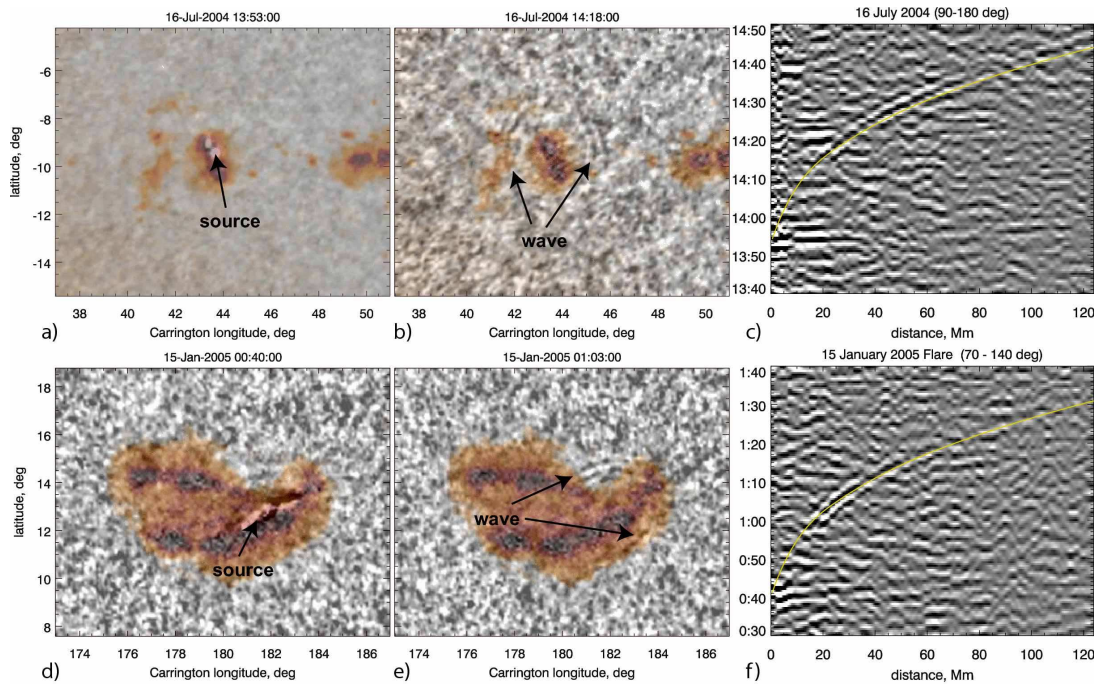


FIGURE 9. Observations of the seismic response of the Sun (“sunquakes”) to two solar flares: a-c) X3 of 16 July, 2004, and d-f) X1 flare of 15 January, 2005. The left panels show a superposition of MDI white-light images of the active regions and locations of the sources of the seismic waves determined from MDI Dopplergrams, the middle column shows the seismic waves, and the right panels show the time-distance diagrams of these events. The thin yellow curves in the right panels represent a theoretical time-distance relation for helioseismic waves for a standard solar model.[37]

Sunquakes

Excitation of Acoustic Waves by Flare Impact

“Sunquakes”, the helioseismic response to solar flares, are caused by strong localized hydrodynamic impacts in the photosphere during the flare impulsive phase. The helioseismic waves are observed directly as expanding circular-shaped ripples in SOHO/MDI Dopplergrams, which can be detected in Dopplergram movies and as a characteristic ridge in time-distance diagrams, [38, 39], or indirectly by calculating integrated acoustic emission [40, 41]. Solar flares are sources of high-temperature plasma and strong hydrodynamic motions in the solar atmosphere. Perhaps, in all flares such perturbations generate acoustic waves traveling through the interior. However, only in some flares the impact is sufficiently localized and strong to produce the seismic waves with the amplitude above the convection noise level. It has been established in the initial July 9, 1996, flare observations [38] that the hydrodynamic impact follows the hard X-ray flux impulse, and hence, the impact of high-energy electrons.

A characteristic feature of the seismic response in this flare and several others [39, 37] is anisotropy of the wave front: the observed wave amplitude is much stronger in

one direction than in the others. In particular, the seismic waves excited during the October 28, 2003, flare had the greatest amplitude in the direction of the expanding flare ribbons. The wave anisotropy was attributed to the moving source of the hydrodynamic impact, which is located in the flare ribbons [39, 42]. The motion of flare ribbons is often interpreted as a result of the magnetic reconnection processes in the corona. When the reconnection region moves up it involves higher magnetic loops, the footpoints of which are further apart. Of course, there might be other reasons for the anisotropy of the wave front, such as inhomogeneities in temperature, magnetic field, and plasma flows. However, the source motion seems to be quite important.

Therefore, we conclude that the seismic wave was generated not by a single impulse but by a series of impulses, which produce the hydrodynamic source moving on the solar surface with a supersonic speed. The seismic effect of the moving source can be easily calculated by convolving the wave Green’s function with a moving source function. The results of these calculations a strong anisotropic wavefront, qualitatively similar to the observations [43]. Curiously, this effect is quite similar to the anisotropy of seismic waves on Earth, when the earthquake rupture moves along the fault. Thus, taking into account the effects of multiple impulses of acceler-

ated electrons and moving source is very important for sunquake theories. The impulsive sunquake oscillations provide unique information about interaction of acoustic waves with sunspots. Thus, these effects must be studied in more detail.

Excitation of Global Oscillations by Sunquakes and Starquakes

An interesting question is if solar and stellar flares can excite global (low-degree) modes of the amplitude detectable by the current telescopes. Baudin and Finidori [44] using the SOHO/GOLF Doppler-shift oscillation data found during the flare of July 9, 1996, when the first "sunquake" was observed in the MDI data the power of solar low-degree modes increased in the frequency range of 3.3 – 3.7 mHz. However, a similar analysis of a stronger flare of October 28, 2003, did not find a significant power increase that would indicate on flare-excited global oscillations (Baudin, private communication). Contrary, a surprisingly strong correlation between increases of the whole-Sun acoustic power in the range of 5-7 mHz observed from the SOHO/VIRGO total irradiance data and the solar soft X-ray flux was found by Karoff and Kjeldsen [45]. They interpreted this correlation as an evidence that solar flares drive global oscillations of the Sun.

To resolve this controversy we estimate an upper amplitude of low-degree solar modes excited by an impulsive impact at the solar surface. The limits on the total momentum and energy of this source can be obtained from the spatially resolved observations of sunquakes.

Indeed, a solution of the non-radial stellar pulsations equation written in symbolic form for a displacement vector ξ :

$$\frac{\partial^2 \xi}{\partial t^2} + \mathcal{L}\xi = 0$$

for initial conditions: $v(r, \theta, \phi, 0) = v_0(r, \theta, \phi)$ can be obtained in terms of normal mode eigenfunctions, $v x_{nlm}$:

$$v(r, \theta, \phi, t) = \sum_{nlm} \frac{\langle \xi_{nlm}^* \cdot v_0 \rangle}{\langle \xi_{nlm}^* \cdot \xi_{nlm} \rangle} \xi_{nlm} \cos(\omega_{nlm} t) e^{-\gamma_{nlm} t},$$

where the angular brackets mean the integration over the solar mass. Assuming that the impact is localized in a very small volume at the surface and calculating the integrals we obtain for the radial component of the oscillation velocity at the surface:

$$v_r(R, \theta, \phi, t) = \sum_{nlm} \frac{P_0}{M_\odot I_{nl}} (2\ell + 1) P_\ell(\cos \theta) \cos(\omega_{nlm} t) e^{-\gamma_{nlm} t},$$

where P_0 is the total momentum of the impact, M_\odot is the solar mass, I_{nl} is the mode inertia, P_ℓ is the Legendre polynomial, ω_{nlm} are the mode eigenfrequencies, and

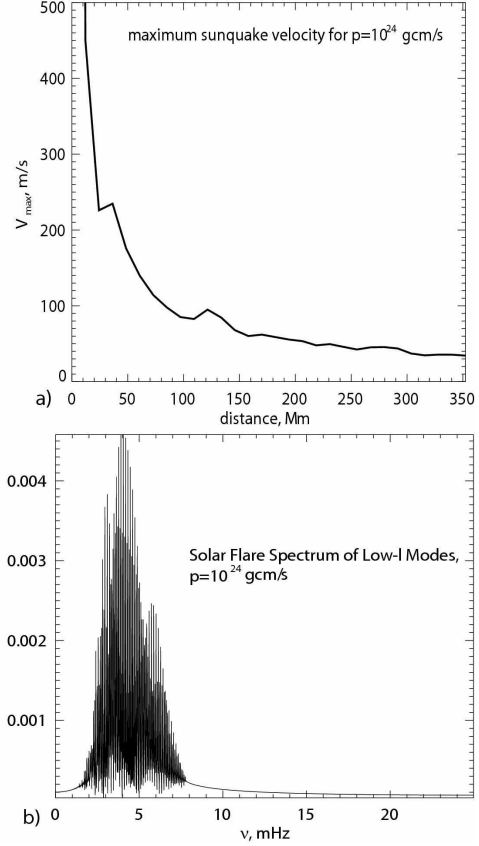


FIGURE 10. a) Theoretical spectrum of solar oscillations excited by an impulsive source of the total momentum of 10^{24} g cm/s. b) The velocity amplitude of low-degree modes $l = 0 - 2$ excited by this source.

γ_{nl} are their damping times. The denominator, $M_\odot I_{nl}$, is often "mode mass". Thus, the mode amplitude excited by the impulsive point source is equal to the total momentum divided by the mode mass and multiplied by a geometrical factor $(2\ell + 1)P_\ell$.

Using this solution we calculate the maximum amplitude of the wave as a function of distance $R\theta$ from the impact (Fig. 10a). For the total momentum 10^{24} g cm/s, the calculated maximum amplitude corresponds to the maximum amplitude observed in the sunquake events [39]. This means that the total momentum of the flare impact does not exceed 10^{24} g cm/s. Then using the same solution we calculate the amplitudes of low- l modes excited by this impact. The velocity spectrum of $l = 0 - 2$ modes is shown in Fig. 10b. The maximum amplitude of these global modes does not exceed 0.4 cm/s. This amplitude is about 100 times smaller than the amplitude of stochastically excited low- l modes. The maximum amplitude of the flare-excited modes is in the frequency range of 4-5 mHz. This is also inconsistent with the suggestion of Karoff and Kjeldsen [45] that

they observed global sunquake oscillations. Perhaps, the high-frequency frequency excess in intensity variations is caused not by oscillations but some other fluctuations in magnetic active regions.

In other stars the situation may be different. The energy of flares on red dwarfs can be 3-4 orders of magnitude higher than on the Sun. It is believed that the physics of these flares is similar to the solar ones. Thus, if the momentum of the flare impact in the stellar photosphere is 3 order of magnitude higher than the amplitude will be also higher by approximately the same amount. This means that the amplitude of global starquake waves can reach 4 m/s and thus can be observable. The oscillations with periods of 3-5 min associated with stellar flares have been observed (e.g. [46]). Perhaps, these were caused by the seismic response and not by coronal loop oscillations as was suggested.

HELIOSEISMIC TOMOGRAPHY

Helioseismic diagnostics based on measurements and inversion of global mode frequencies are well-known (e.g. [47, 2]). Most recent effort in helioseismic applications has been focused on local techniques. Helioseismic tomography (or time-distance helioseismology) is one of these.

Basic Principles of Helioseismic Tomography

The basic idea of helioseismic tomography is to measure the acoustic travel time between different points on the solar surface, and then to use these measurement for inferring variations of the structure and flow velocities in the interior along the wave paths connecting the surface points. This idea is similar to the Earth's seismology. However, unlike in Earth, the solar waves are generated stochastically by numerous acoustic sources in the subsurface layer of turbulent convection. Therefore, the wave travel times are determined from the cross-covariance function, $\Psi(\tau, \Delta)$, of the oscillation signal, $f(t, \vec{r})$, between different points on the solar surface [16]:

$$\Psi(\tau, \Delta) = \int_0^T f(t, \vec{r}_1) f^*(t + \tau, \vec{r}_2) dt, \quad (1)$$

where Δ is the angular distance between the points with coordinates \vec{r}_1 and \vec{r}_2 , τ is the delay time, and T is the total time of the observations. Because of the stochastic nature of excitation of the oscillations, function Ψ must be averaged over some areas on the solar surface to achieve a signal-to-noise ratio sufficient for measuring travel times τ . The oscillation signal, $f(t, \vec{r})$, is usu-

ally the Doppler velocity or intensity. A typical cross-covariance function shown in Fig. 11 displays two sets of ridges which correspond to the first and second bounces of acoustic wave packets from the surface.

The cross-covariance function represents a solar 'seismogram'. Ideally, the seismogram should be inverted to infer the structure and flows using a wave theory. However, in practice, as in terrestrial seismology different approximations are employed, the most simple and powerful of which is the geometrical acoustic (ray) approximation.

Generally, the observed solar oscillation signal corresponds to radial displacement or pressure perturbation, and can be represented in terms of normal modes, or standing waves:

$$f(t, r, \theta, \phi) = \sum_{nlm} a_{nlm} \xi_{nlm}(r, \theta, \phi) \exp(i\omega_{nlm}t + i\phi_{nlm}), \quad (2)$$

where n, l and m are the radial order, angular degree and angular order of a normal mode respectively, $\xi_{nlm}(r, \theta, \phi)$ is a mode eigenfunction in spherical coordinates, r, θ and ϕ , ω_{nlm} is the eigenfrequency, and ϕ_{nlm} is an initial phase of the mode. Using eq. (1), the cross-covariance function can be expressed in terms of normal modes, and then represented as a superposition of traveling wave packets. An example of the theoretical cross-covariance function of p modes of the standard solar model in Fig. 11.

By grouping the modes in narrow ranges of the angular phase velocity, $v = \omega_{nl}/L$, where $L = \sqrt{l(l+1)}$, and applying the method of stationary phase, the cross-covariance function can be approximately represented in the form [50]:

$$\Psi(\tau, \Delta) \propto \sum_{\delta v} \cos \left[\omega_0 \left(\tau - \frac{\Delta}{v} \right) \right] \exp \left[-\frac{\delta \omega^2}{4} \left(\tau - \frac{\Delta}{u} \right)^2 \right], \quad (3)$$

where δv is a narrow interval of the phase speed, $u \equiv (\partial \omega / \partial k_h)$ is the horizontal component of the group velocity, $k_h = 1/L$ is the angular component of the wave vector, and ω_0 is the central frequency of a Gaussian frequency filter applied to the data, and $\delta \omega$ is the characteristic width of this filter. Therefore, the phase and group travel times are measured by fitting individual terms of eq. (3) to the observed cross-covariance function using a least-squares technique. In some cases the ridges of the cross-covariance function may partially overlap, thus making the interpretation of the time-distance results more difficult.

This technique measures both phase (Δ/v) and group (Δ/u) travel times of the p-mode wave packets. It was found that the noise level in the phase-time measurements is substantially lower than in the group-time measurements. The geometrical acoustic (ray) approximation was employed to relate the measured phase times to the

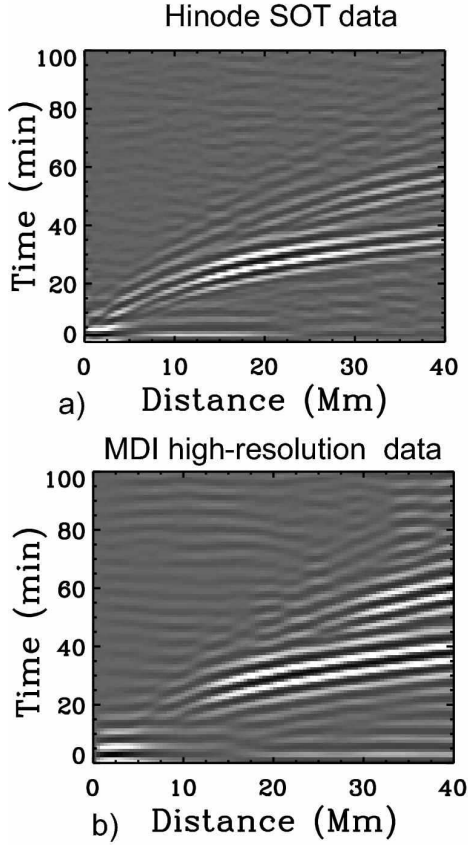


FIGURE 11. Cross-covariance functions of solar oscillations (time-distance diagrams) obtained from a) Hinode and b) MDI high-resolution data.[48]

internal properties of the Sun. More precisely, the variations of the local travel times at different points on the surface, relative to the travel times averaged over the observed area are measured. Then variations of the internal structure and flow velocities are inferred from the travel time anomalies using a perturbation theory.

High-resolution Helioseismology from Hinode

Solar Optical Telescope (SOT) [27] on Hinode spacecraft [26] has unique capabilities for high-resolution helioseismology. The high-resolution helioseismology investigations are at the very beginning and undoubtedly will bring new understanding of the subsurface structure and dynamics, particularly, of the magnetized plasma of sunspots and active regions. The unique advantage of Hinode observation is clearly seen by comparing the time-distance diagrams (cross-covariance functions) obtained from Hinode and SOHO/MDI data (Fig. 11). For

the MDI data, the time-distance ridges corresponding to signals of traveling wave packets, are not resolved for distances shorter than 5-10 Mm. The cross-covariance signal at these distances is dominated by horizontal artifact ridges (in the lower left corners of Figs 11b). In the time-distance diagram obtained from Hinode data (Fig. 11a) the wave signal is resolved for much shorter travel distances, up to about 2 Mm. This is comparable with the characteristic wavelength of solar oscillations.

In Figure 12 we compare subsurface structures and flows below sunspots obtained from Hinode and MDI data. A vertical cut along the East-West direction approximately in the middle of a large sunspot observed in AR 10953, May 2, 2007, (Fig. 12b), shows that the wave speed anomalies extend about half of the sunspot size beyond the sunspot penumbra into the plage area. In the vertical direction, the negative wave speed perturbation extends to a depth of 3–4 Mm. The positive perturbation is about 9 Mm deep, but it is not clear whether it extends further, because our inversion cannot reach deeper layers because of the small field of view. Similar two-layer sunspot structures were observed before from SOHO/MDI [51](Fig. 12a). But, it is striking that the new images strongly indicate on the cluster structure of the sunspot. This was not previously seen in the tomographic images of sunspots obtained with lower resolution. The high-resolution flow field below the sunspot is also significantly more complicated than the previously inferred from SOHO/MDI [52] (Fig. 12c), but reveals the same general converging downdraft pattern. A vertical view of an averaged flow field (Fig. 12d) shows nicely the flow structure beneath the active region. Strong downdrafts are seen immediately below the sunspot's surface, and extends up to 6 Mm in depth. A little beyond the sunspot's boundary, one can find both upward and inward flows. Clearly, large-scale mass circulations form outside the sunspot, bringing plasma down along the sunspot's boundary, and back to the photosphere within about twice of the sunspot's radius. It is remarkable that such an apparent mass circulation is obtained directly from the helioseismic inversions without using any additional constraints, such as forced mass conservation. Previously, the circulation pattern was not that clear.

CONCLUSION

During the past decade thanks to the long-term continuous observations from the ground and space the physics of solar oscillations made a tremendous progress in understanding the excitation mechanisms in various condition of the quiet Sun and active regions, wave propagation and their interaction with magnetic fields and turbulence, and in developing new techniques for helioseismic diagnostics of the solar structure and dynam-

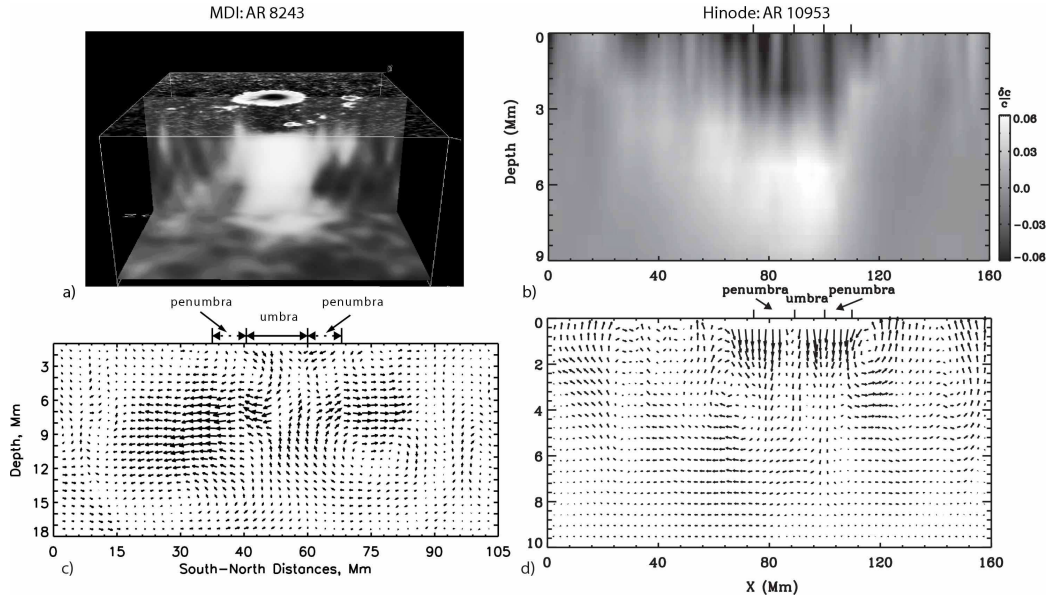


FIGURE 12. Wave speed perturbations($a - b$) and flow velocities ($c - d$) beneath sunspots from the MDI (*left*) and Hinode (*right*) data [49].

ics. However, many problems are still unresolved. Most of them are related to phenomena in magnetic field regions. In particular, in sunspots 3-min oscillations and running penumbra waves remain a mystery. The excitation and damping mechanisms in the turbulent magnetized plasma of active regions are far from understanding. The processes of wave scattering and transformation must be studied in realistic conditions of the upper convection zone and solar atmosphere. The prime helioseismology tasks are to detect processes of magnetic field generation and transport in the solar interior, and formation of active regions and sunspots. This will help to understand the physics of the solar dynamo and the cyclic behavior of solar activity.

For solving these tasks it is very important to continue developing realistic MHD simulations of solar convection and oscillations and to obtain continuous high-resolution helioseismology data for the whole Sun. The recent observations from Hinode have convincingly demonstrated advantages of high-resolution helioseismology, but unfortunately such data are available only for small regions and for short periods of time. A new substantial progress in observations of solar oscillations is expected from the Solar Dynamics Observatory (SDO) space mission scheduled for launch in December 2009. The Helioseismic and Magnetic Imager (HMI) instrument on SDO will provide uninterrupted Doppler shift measurements over the whole visible disk of the Sun with a spatial resolution of 0.5 arcsec per pixel (4096×4096 images) and 40-50 sec time cadence. The total amount of data from this instrument will reach 2 Tb per day. This

tremendous amount of data will be processed through a specially developed data analysis pipeline and will provide high-resolution maps of subsurface flows and sound-speed structures [53]. These data will enable investigations of the multi-scale dynamics and magnetism of the Sun and also contribute to our understanding of the Sun as a star.

REFERENCES

1. R. B. Leighton, R. W. Noyes, and G. W. Simon, *Astrophys. J.* **135**, 474 (1962).
2. J. Christensen-Dalsgaard, *Reviews of Modern Physics* **74**, 1073–1129 (2002).
3. P. Ledoux, and T. Walraven, *Handbuch der Physik* **51**, 353–604 (1958).
4. J. Zhao, T. Hartlep, A. G. Kosovichev, and N. N. Mansour, *ArXiv e-prints* (2009).
5. W. J. Chaplin, G. Houdek, Y. Elsworth, D. O. Gough, G. R. Isaak, and R. New, *Mon. Not. Roy. Astron. Soc.* **360**, 859–868 (2005).
6. R. Nigam, and A. G. Kosovichev, *Astrophys. J. Lett.* **505**, L51 (1998).
7. A. C. Birch, and A. G. Kosovichev, *Solar Phys.* **192**, 193–201 (2000).
8. A. C. Birch, A. G. Kosovichev, and T. L. Duvall, Jr., *Astrophys. J.* **608**, 580–600 (2004).
9. S. P. Rajaguru, A. C. Birch, T. L. Duvall, Jr., M. J. Thompson, and J. Zhao, *Astrophys. J.* **646**, 543–552 (2006).
10. K. V. Parchevsky, J. Zhao, and A. G. Kosovichev, *Astrophys. J.* **678**, 1498–1504 (2008).
11. F. Baudin, R. Samadi, M.-J. Goupil, T. Appourchaux,

- C. Barban, P. Boumier, W. J. Chaplin, and P. Gouttebroze, *Astron. Astrophys.* **433**, 349–356 (2005).
12. L. Jacoutot, A. G. Kosovichev, A. A. Wray, and N. N. Mansour, *Astrophys. J.* **682**, 1386–1391 (2008).
 13. T. R. Rimmele, P. R. Goode, E. Harold, and R. T. Stebbins, *Astrophys. J. Lett.* **444**, L119–L122 (1995).
 14. R. Skartlien, R. F. Stein, and Å. Nordlund, *Astrophys. J.* **541**, 468–488 (2000).
 15. R. F. Stein, and Å. Nordlund, *Astrophys. J.* **546**, 585–603 (2001).
 16. T. L. Duvall, Jr., S. M. Jefferies, J. W. Harvey, Y. Osaki, and M. A. Pomerantz, *Astrophys. J.* **410**, 829–836 (1993).
 17. T. Toutain, T. Appourchaux, C. Frohlich, A. Kosovichev, N. Rakesh, and P. Scherrer, “Line Asymmetry of VIRGO and MDI Low-Degree p Modes,” in *Structure and Dynamics of the Interior of the Sun and Sun-like Stars*, edited by S. Korzennik, 1998, vol. 418 of *ESA Special Publication*, p. 973.
 18. M. Gabriel, *Astron. Astrophys.* **265**, 771–780 (1992).
 19. R. Nigam, A. G. Kosovichev, P. H. Scherrer, and J. Schou, *Astrophys. J. Lett.* **495**, L115 (1998).
 20. U. Mitra-Kraev, A. G. Kosovichev, and T. Sekii, *Astron. Astrophys.* **481**, L1–L4 (2008).
 21. K. V. Parchevsky, and A. G. Kosovichev, *Astrophysical Journal* **666**, L53–L56 (2007).
 22. I. W. Roxburgh, and S. V. Vorontsov, *Mon. Not. Roy. Astron. Soc.* **292**, L33–L36 (1997).
 23. G. Severino, M. Magrì, M. Oliviero, T. Straus, and S. M. Jefferies, *Astrophys. J.* **561**, 444–449 (2001).
 24. R. Wachter, and A. G. Kosovichev, *Astrophys. J.* **627**, 550–561 (2005).
 25. D. Georgobiani, R. F. Stein, and Å. Nordlund, *Astrophys. J.* **596**, 698–701 (2003).
 26. T. Kosugi, K. Matsuzaki, T. Sakao, T. Shimizu, Y. Sone, S. Tachikawa, T. Hashimoto, K. Minesugi, A. Ohnishi, T. Yamada, S. Tsuneta, H. Hara, K. Ichimoto, Y. Suematsu, M. Shimojo, T. Watanabe, S. Shimada, J. M. Davis, L. D. Hill, J. K. Owens, A. M. Title, J. L. Culhane, L. K. Harra, G. A. Doschek, and L. Golub, *Solar Phys.* **243**, 3–17 (2007).
 27. S. Tsuneta, K. Ichimoto, Y. Katsukawa, S. Nagata, M. Otsubo, T. Shimizu, Y. Suematsu, M. Nakagiri, M. Noguchi, T. Tarbell, A. Title, R. A. Shine, W. Rosenberg, C. Hoffmann, B. Jurcevich, G. Kushner, M. Levay, B. Lites, D. Elmore, T. Matsushita, N. Kawaguchi, H. Saito, I. Mikami, L. D. Hill, and J. K. Owens, *Solar Phys.* **249**, 167–196 (2008).
 28. K. Nagashima, T. Sekii, A. G. Kosovichev, H. Shibahashi, S. Tsuneta, K. Ichimoto, Y. Katsukawa, B. Lites, S. Nagata, T. Shimizu, R. A. Shine, Y. Suematsu, T. D. Tarbell, and A. M. Title, *Pub. Astron. Soc. Japan* **59**, 631 (2007).
 29. T. L. Duvall, Jr., A. G. Kosovichev, and K. Murawski, *Astrophys. J. Lett.* **505**, L55 (1998).
 30. D. C. Braun, T. L. Duvall, Jr., and B. J. Labonte, *Astrophys. J. Lett.* **319**, L27–L31 (1987).
 31. P. S. Cally, *Mon. Not. Roy. Astron. Soc.* **395**, 1309–1318 (2009).
 32. K. V. Parchevsky, and A. G. Kosovichev, *Astrophys. J.* **694**, 573–581 (2009).
 33. M. Schüssler, and A. Vögler, *Astrophys. J. Lett.* **641**, L73–L76 (2006).
 34. B. W. Lites, “Sunspot oscillations - Observations and implications,” in *NATO ASIC Proc. 375: Sunspots. Theory and Observations*, edited by J. H. Thomas, and N. O. Weiss, 1992, pp. 261–302.
 35. D. C. Braun, C. Lindsey, Y. Fan, and S. M. Jefferies, *Astrophys. J.* , **392**, 739 (1992).
 36. L. Jacoutot, A. G. Kosovichev, A. Wray, and N. N. Mansour, *Astrophys. J. Lett.* **684**, L51–L54 (2008).
 37. A. G. Kosovichev, “Sunquake sources and wave propagation,” in *Proceedings of SOHO 18/GONG 2006/HELAS I, Beyond the spherical Sun*, 2006, vol. 624 of *ESA Special Publication*.
 38. A. G. Kosovichev, and V. V. Zharkova, *Nature* **393**, 317–318 (1998).
 39. A. G. Kosovichev, *Solar Phys.* **238**, 1–11 (2006).
 40. A.-C. Donea, D. C. Braun, and C. Lindsey, *Astrophys. J. Lett.* **513**, L143–L146 (1999).
 41. A.-C. Donea, and C. Lindsey, *Astrophys. J.* **630**, 1168–1183 (2005).
 42. A. G. Kosovichev, “Direct Observations of Acoustic Waves Excited by Solar Flares and their Propagation in Sunspot Regions,” in *Solar MHD Theory and Observations: A High Spatial Resolution Perspective*, edited by J. Leibacher, R. F. Stein, and H. Uitenbroek, 2006, vol. 354 of *Astronomical Society of the Pacific Conference Series*, p. 154.
 43. A. G. Kosovichev, *Astrophys. J. Lett.* **670**, L65–L68 (2007).
 44. F. Baudin, and H. Finidori, “Looking for Correlated Excitation of Solar P Modes,” in *SOHO 14 Helio- and Asteroseismology: Towards a Golden Future*, edited by D. Danesy, 2004, vol. 559 of *ESA Special Publication*, p. 51.
 45. C. Karoff, and H. Kjeldsen, *Astrophys. J. Lett.* **678**, L73–L76 (2008).
 46. M. Mathioudakis, J. H. Seiradakis, D. R. Williams, S. Avgoloupis, D. S. Bloomfield, and R. T. J. McAteer, *Astron. Astrophys.* **403**, 1101–1104 (2003).
 47. A. G. Kosovichev, *Journal of Computational and Applied Mathematics* **109**, 1–39 (1999).
 48. T. Sekii, A. G. Kosovichev, J. Zhao, S. Tsuneta, H. Shibahashi, T. E. Berger, K. Ichimoto, Y. Katsukawa, B. Lites, S. Nagata, T. Shimizu, R. A. Shine, Y. Suematsu, T. D. Tarbell, and A. M. Title, *Pub. Astron. Soc. Japan* **59**, 637 (2007).
 49. J. Zhao, J., A. G. Kosovichev, and T. Sekii, *Astrophys. J.* **submitted** (2009).
 50. A. G. Kosovichev, and T. L. Duvall, Jr., “Acoustic tomography of solar convective flows and structures,” in *SCORE’96 : Solar Convection and Oscillations and their Relationship*, edited by F. P. Pijpers, J. Christensen-Dalsgaard, and C. S. Rosenthal, 1997, vol. 225 of *Astrophysics and Space Science Library*, pp. 241–260.
 51. A. G. Kosovichev, T. L. . J. Duvall, and P. H. Scherrer, *Solar Phys.* **192**, 159–176 (2000).
 52. J. Zhao, A. G. Kosovichev, and T. L. Duvall, Jr., *Astrophys. J.* **557**, 384–388 (2001).
 53. A. G. Kosovichev, and T. L. Duvall, *Space Science Reviews* **124**, 1–4 (2006).